

# Producing Bessel Beams with an RF Transformer

Jian-yu Lu <sup>1</sup>

<sup>1</sup>Affiliation not available

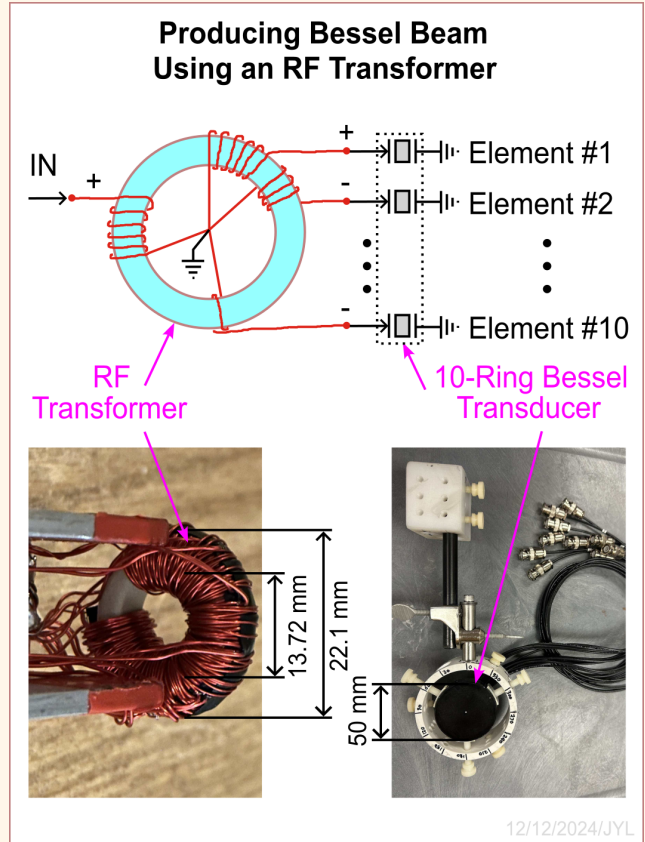
March 28, 2025

# Producing Bessel Beams with an RF Transformer

Jian-yu Lu, *Life Fellow, IEEE*

**Abstract**— Bessel beams are exact solutions to the isotropic/homogeneous wave equation. In theory, they can propagate to infinite distance without diffraction. In practice, when produced with a finite aperture, they have a very large depth of field, i.e., they can maintain a small beamwidth over a large distance. In addition, they have a self-healing ability after encountering an obstacle. Because of these properties, Bessel beams have applications in optics, electromagnetics, ultrasound, quantum communications, electron beam guidance, and so on. Previously, in ultrasound, Bessel beams were produced with an annular array transducer driven by multiple independent high-voltage radio-frequency (RF) power amplifiers that were bulky and consume a lot of power, which limits the Bessel beams in applications such as wearable medical ultrasound imaging and wearable super-resolution imaging. In this paper, pulse (broadband) Bessel beams were produced by single high-voltage RF power amplifier in combination with an RF transformer, reducing the power consumption, size, and weight. Experiments were performed to produce the pulse Bessel beams in water with a custom RF transformer and a custom 10-ring, 50-mm diameter, 2.5-MHz center frequency, and broadband (about 72% -6-dB relative one-way bandwidth) 1-3 lead zirconate titanate (PZT) ceramic/polymer composite annular array transducer driven by a commercial RF power amplifier at about  $\pm 90$  V. The results show that the pulse Bessel beams produced were very close to those produced with 10 independent high-voltage RF power amplifiers, and the pulse Bessel beams had a -6-dB beamwidth of about 2.53 mm (4.22 wavelengths) and a depth of field that is close to a theoretical prediction of about 216 mm (360 wavelengths). The reduced number of high-voltage RF power amplifiers makes it easier to apply Bessel beams to wearable medical ultrasound imaging or wearable super-resolution imaging.

**Index Terms**— Bessel beams, depth of field, electromagnetic, medical imaging, optics, radio frequency (RF), RF power amplifier, RF transformer, super-resolution imaging, ultrasound, ultrasound imaging, wearable imaging.



## I. INTRODUCTION

BESSEL beams are exact solutions to the isotropic/homogeneous wave equation. They were first obtained by Julius A. Stratton in his book in 1941 [1]. In 1987, Durnin et al. studied the Bessel beams and performed an experiment in optics to produce these beams [2]-[4]. In theory, Bessel beams can propagate to infinite distance without lateral spreading of the beams (diffraction free). In practice, when realized with a finite aperture, these beams

have a large depth of field (maintaining a small beamwidth over a large distance) [5]. In addition, these beams can heal themselves (self healing) after encountering an obstacle [6]. Because of these properties, Bessel beams have many applications in, for example, medical ultrasound imaging [5][7]-[8], optical imaging (such as optical coherence tomography or OCT) [9], photoacoustic imaging [10], blood flow velocity vector imaging [11], tissue property identifications [12], nondestructive evaluations (NDE) of materials [13], construction of new beams by orthogonal bases [14], ultrasound therapy [15], acoustical [16] and optical [17] trapping of small particles over a large distance without losing focus, acoustic holograms [18], super-resolution optical imaging [19], optical light-sheet microscopy [20], optical

Jian-yu Lu is with the Department of Bioengineering, The University of Toledo, Toledo, Ohio 43606, USA. (e-mail: jian-yu.lu@ieee.org).

### Highlights

- **A radio-frequency (RF) transformer in combination with single RF power amplifier was used to drive an annular array transducer to produce pulse Bessel beams that have a very large depth of field.**
- **Experiments were performed and the results show that the method can produce pulse Bessel beams that were very close to those produced traditionally with multiple RF power amplifiers.**
- **The reduced number of high-voltage RF power amplifiers makes it easier to apply the Bessel beams to wearable medical ultrasound imaging and wearable super-resolution imaging.**

material processing such as precision laser cutting [21], optical communications that resist turbulence [22], quantum communications [23], quantum entanglement [24][25], electron beam guidance [26], laser-driven accelerators [27], and electromagnetic waves [28].

Bessel beams can be produced by various methods. For example, in optics, Axicon Lens was used to produce Bessel beams approximately in a certain range away from the lens (the sidelobes of the beams are high near the surface of the lens and the intensity of the beam is not constant over the distance) [29]. Fourier method was used to produce Bessel beams [30]. In this method, a ring mask was placed at the focal distance of a lens and a Bessel beam was produced by a Fourier transform of the ring that was illuminated by a plane wave. However, this method has low energy efficiency since only a small amount of light can pass through the narrow ring slit. Spiral phase plate (SPP) was used to produce spiral or vortex Bessel beams [31] that are similar to the higher-order Bessel beams (see Eq. 10 in Ref. [32]). However, the intensity of such beams is zero on the beam axis [5]. Spatial light modulator (SLM) with certain phase profiles was used to produce Bessel beams [33]. However, such device requires a complicated system to operate and the accuracy of the produced Bessel beams is limited. Bessel beams also can be produced by nonlinear effects where the amplitude can alter the phase of the wave [34]. This method relies on nonlinear properties of propagating media and thus its applications are limited. In addition, Bessel beams can be produced by coupling a specific mode of waves into an optical fiber or a waveguide [35]. However, such a method only produces the Bessel beams in a confined space.

In acoustics or ultrasound, there are also many methods to produce Bessel beams [5][36]. For example, A 2.5-MHz, 50-mm diameter, and 10-ring (the ring widths and positions were determined by those of the lobes of a Bessel function) ultrasound annular array transducer (made of 1-3 lead zirconate titanate (PZT) ceramic/polymer composite material) was used to produce a zeroth-order Bessel beam for medical imaging in 1990 [5]. Also, a 2.25-MHz piezoelectric ceramic transducer poled nonuniformly in radial direction was used to produce a zeroth-order Bessel beam [37]. The construction of such transducer was complicated and, unlike the annular array transducer, it could not be used to produce different transmit and receive beams to reduce sidelobes. The optical Axicon above was adapted to ultrasound to produce quasi Bessel beams [38][39]. Holographic phase plates were used to produce Bessel beams [18]. However, this method works only in a narrower bandwidth since the phase shifts required are

frequency dependent. Metamaterials have been used to make a lens to produce an 8-KHz quasi Bessel beam in the air in a computer simulation [40]. This approach was similar to that of an Axicon except that a point source was used to illuminate the lens made of metamaterials to form an Axicon wavefront to produce a Bessel beam approximately. In addition, a two-dimensional (2D) array transducer was studied to produce and steer Bessel beams for pulse-echo medical imaging [41]. However, a 2D array transducer is expensive and requires complicated wiring and associated electronics.

Although various methods can be used to produce Bessel beams, for medical ultrasound imaging, the approach that uses an annular array transducer is most attractive since it has several advantages [5]. First, by setting the widths and positions of the rings of an annular array transducer to be corresponding to those of the lobes of a Bessel function, the number of rings can be minimized (see the 10-ring annular array transducer in Ref. [5]) and thus the array is relatively simple to construct and wire. As a comparison, a 128x128 2D array transducer has 16,384 elements, and even a one-dimensional (1D) array transducer typically has 128 to 256 elements. Despite the 10-ring, 2.5-MHz, and 50-mm diameter annular array transducer has a relatively small number of elements, it can be used to produce good Bessel beams of about 2.53-mm (4.22 wavelengths) -6-dB beamwidth over a very large depth of field of about 216 mm (360 wavelengths) in water [5]. Second, Bessel beams produced by an annular array transducer can be broadband (i.e., they can have a short pulse length), which is important for a high axial resolution in pulse-echo imaging. Also, the lateral beamwidth (related to the image lateral resolution) of the Bessel beams produced with an annular array transducer is independent of the pulse length over a large depth of field. Third, the energy efficiency of producing Bessel beams with an annular array transducer is higher than that with a single-ring transducer since the active surface area of the annular array transducer is larger. Higher energy efficiency increases signal-to-noise ratio (SNR) and the penetration depth of the beams in objects such as the biological soft tissues. Fourth, the amplitude and phase of the signal of each ring of the annular array transducer can be easily controlled to produce different beams. For example, the annular array transducer can be used to produce a Bessel beam in both transmit and receive to maintain a uniform beamwidth or lateral resolution in a pulse-echo imaging, or it can be used to produce a Bessel beam in transmit and then be apodized in aperture to produce a dynamically focused beam such as a dynamically focused Gaussian beam in receive to reduce the sidelobes of the transmit Bessel beam and increase

image contrast [5][7]. Fifth, the annular array transducer can produce Bessel beams starting from the surface of the transducer until the depth of field of the beams. This allows objects that are very close to the surface of the transducer to be imaged.

Despite the advantages of producing Bessel beams with an annular array transducer, previously, each ring of the transducer was independently driven by a high-voltage radio-frequency (RF) power amplifier, consuming a lot of power since multiple such amplifiers were needed to drive the transducer [5]. Because of high power and high voltage, to avoid overheating and voltage breakdown, these amplifiers were bulky (had a large physical size and heavy weight), which limits the Bessel beams in wearable applications (devices could be battery operated and worn on the human body for an extended period of time) such as wearable medical ultrasound imaging [42]-[43] and wearable super-resolution imaging [44]-[46]. To reduce the power consumption, size, and weight, it is desired to use single high-voltage RF power amplifier to produce Bessel beams. However, single power amplifier can normally drive a single-element transducer that can only focus at a fixed depth with a small depth of field, especially when the  $f$ -number (the focal distance divided by the transducer diameter) of the transducer is small. Outside the depth of field, the image quality is degraded quickly.

To address the issues above, in this paper, a method that uses single high-voltage RF power amplifier in combination with an RF transformer to produce Bessel beams was developed. In the method, the single RF power amplifier was used to drive the primary winding of the RF transformer that had 10 secondary windings connected to respective 10 rings of the annular array transducer mentioned above. The number of turns of each secondary winding was proportional to the absolute value of the peak of the corresponding lobe of a Bessel function and the phase of the winding (direction of winding) was determined by the sign of the peak (notice that only two phases,  $0^\circ$  and  $180^\circ$ , are needed to produce a Bessel beam) [5]. Since the size of the RF transformer can be small and only single high-voltage RF power amplifier is needed in the method, the overall size, weight, and power consumption of the electronics can be significantly reduced, making it easier to apply the Bessel beams to wearable applications such as wearable medical ultrasound imaging [42]-[43] and wearable super-resolution imaging [44]-[46]. In addition, the RF transformer naturally helps its electrical impedance matching with the annular array transducer. Notice that since both the absolute value of the peak of the lobes of a Bessel function and the number of turns of each secondary winding of the RF transformer are proportional to  $1/\sqrt{r}$  asymptotically, where  $r$  is the radial distance, the electrical impedances of both the secondary windings and the corresponding rings of the annular array transducer will be proportional to  $1/r$  for outer rings. This is because the electrical impedance of a ring of an annular array transducer is inversely proportional to the area of the ring (assuming that a ring of the annular array transducer is bounded by radii  $r_1$  and  $r_2 > r_1$ , its area will be  $\pi(r_2^2 - r_1^2) = \pi(r_2 + r_1)(r_2 - r_1) \approx$

$2\pi r(\Delta r)$  or is proportional to  $r$  since  $\Delta r$  is almost a constant and  $r_1 \approx r_2 \approx r$  if  $r$  is not too small). To form an image, the annular array transducer can be scanned linearly or in a sector format using methods such as a linear stage, a wobbler [47]-[48], or moving reflectors [49]-[50]. The images produced can be real-time, have a large depth of field, and have a strong self-healing ability (reduce shadows caused by objects such as hard tumors) [6][51].

The paper is organized as follows. The theory of Bessel beams is given in Section II. The experiment methods are in Section III. The results are in Section IV. Finally, a discussion and a conclusion are given in Sections V and VI respectively.

## II. THEORETICAL PRELIMINARY

The free space (or isotropic/homogeneous) scalar wave equation in cylindrical coordinates is given by:

$$\left[ \frac{1}{r} \frac{\partial}{\partial r} \left( r \frac{\partial}{\partial r} \right) + \frac{1}{r^2} \frac{\partial^2}{\partial \phi^2} + \frac{\partial^2}{\partial z^2} - \frac{1}{c^2} \frac{\partial^2}{\partial t^2} \right] \Phi(r, \phi, z; t) = 0, \quad (1)$$

where  $r = \sqrt{x^2 + y^2}$  represents the radial coordinate,  $\phi$  is an azimuthal angle,  $z$  is an axial axis that is perpendicular to the plane defined by  $r$  and  $\phi$ ,  $\vec{r} = (r \cos(\phi), r \sin(\phi), z)$  represents a spatial position,  $t$  is the time,  $c$  is the speed of sound or light, and  $\Phi(r, \phi, z; t)$  (wave field) represents acoustic pressure or Hertz potential that is a function of  $r$ ,  $\phi$ ,  $z$ , and  $t$ .

From Eq. (1), a family of solutions to the wave equation can be obtained (see Eq. (2) in Ref. [32]):

$$\Phi_\zeta(s) = \int_0^\infty T(k) \left[ \frac{1}{2\pi} \int_{-\pi}^\pi A(\theta) g(s) d\theta \right] dk, \quad (2)$$

where

$$s = \alpha_0(k, \zeta) r \cos(\phi - \theta) + b(k, \zeta) [z \pm c_1(k, \zeta) t], \quad (3)$$

and where

$$c_1(k, \zeta) = c \sqrt{1 + [\alpha_0(k, \zeta) / b(k, \zeta)]^2}, \quad (4)$$

where  $k$ ,  $\zeta$ , and  $\theta$  are parameters that are independent of the spatial positions,  $\zeta$  is an Axicon angle [38][52],  $T(k)$  is any complex function (well behaved) of  $k$  and could include the temporal frequency transfer function of a wave source,  $A(\theta)$  is any complex function (well behaved) of  $\theta$  and represents a weighting function of the integration with respect to  $\theta$ ,  $g(s)$  is any complex function (well behaved) of  $s$ , and both  $\alpha_0(k, \zeta)$  and  $b(k, \zeta)$  are any complex functions of  $k$  and  $\zeta$ . Notice that " $\pm$ " in Eq. (3) represent backward and forward propagating waves, respectively. (In the following, we consider only the forward propagating waves.)

If  $T(k) = \delta(k - k_0)$ , where  $\delta(k - k_0)$  is a Dirac-Delta function [53],  $k_0 = \omega_0 / c > 0$  is a constant that represents a wave number,  $\omega_0 = 2\pi f_0$  is an angular frequency,  $f_0$  is the frequency of the wave,  $g(s) = e^s$ ,  $\alpha_0(k, \zeta) = -i\alpha$ ,

$b(k, \zeta) = i\beta = i\omega_0 / c_1$ ,  $i = \sqrt{-1}$ , from Eqs. (2) and (3), one obtains Durnin's beam [2] (see Eq. (8) in Ref. [32]):

$$\Phi_D(s) = \left[ \frac{1}{2\pi} \int_{-\pi}^{\pi} A(\theta) e^{-i\alpha r \cos(\phi-\theta)} d\theta \right] e^{i(\beta z - \alpha_0 t)}, \quad (5)$$

where

$$\beta = \sqrt{k_0^2 - \alpha^2}, \quad (6)$$

and where  $\alpha$  is a constant and is a scaling parameter of the beam.

Notice that since the integration in the square bracket in Eq. (5) is independent of the propagation distance,  $z$ , and the time,  $t$ , in theory, Durnin's beam does not spread or diffract in the transverse plane  $(r, \phi)$  as the wave propagates to an infinite distance. However, since  $c_1(k_0, \zeta) = \omega_0 / \beta$ , the speed of wave of Durnin's beam in Eq. (5) depends on the wave number,  $k_0$ . Therefore, if  $T(k)$  in Eq. (2) is a complex function containing multiple frequencies,  $\Phi_\zeta(s)$  will represent a dispersive wave (wave speed changes with the frequency) and its shape will change in the axial direction,  $z$ , as the wave propagates. To get waves that do not diffract in both transverse and axial directions as they propagate to an infinite distance,  $c_1(k_0, \zeta)$  in Eq. (2) must be a constant. X waves [32] or quantum X waves [54][55] are such waves that have a constant speed  $c_1 \geq c$ , i.e., both the phase and group velocities of these waves are the same and are always larger than or equal to the speed of light in vacuum or the speed of sound in isotropic/homogeneous media.

If  $A(\theta) = i^n e^{in\theta}$ , we obtain the  $n$ th-order Bessel beams (see Eq. (10) in Ref. [32]):

$$\Phi_{J_n}(s) = J_n(\alpha r) e^{i(\beta z - \alpha_0 t + n\phi)}, \quad n = 0, 1, 2, \dots, \quad (7)$$

where  $J_n(\cdot)$  is the  $n$ th-order Bessel function of the first kind. Because the  $n$ th-order Bessel beam in Eq. (7) is zero on the beam axis unless  $n=0$ , in the remainder of this paper, we will only study the zeroth-order Bessel beam  $J_0$  that is axially symmetric (i.e., not a function  $\phi$ ) and can be applied to medical imaging [5]:

$$\Phi_{J_0}(r, z) = J_0(\alpha r) e^{i(\beta z - \alpha_0 t)}. \quad (8)$$

If  $\alpha = 0$ , Eq. (8) represents a plane wave [2].

### III. METHODS

#### A. Bessel Transducer

To produce a Bessel beam experimentally, a custom 10-ring, 2.5-MHz center frequency, broadband (about 72% -6dB relative one-way bandwidth), and 50-mm diameter annular array transducer (Bessel transducer) was used [5]. The transducer was made of 1-3 PZT ceramic/polymer composite material sandwiched between front matching (matched to water) and back absorbing layers. The width of each ring is proportional to that of the corresponding lobe of the  $J_0(\alpha r)$  Bessel function, where  $\alpha = 1202.45 \text{ m}^{-1}$ . The gap between

adjacent rings is about 0.2 mm. The radii of the centers of the gaps were set to be at the corresponding zeros of the  $J_0(\alpha r)$  Bessel function. A photo of the annular array transducer is shown in Fig. 1(c).

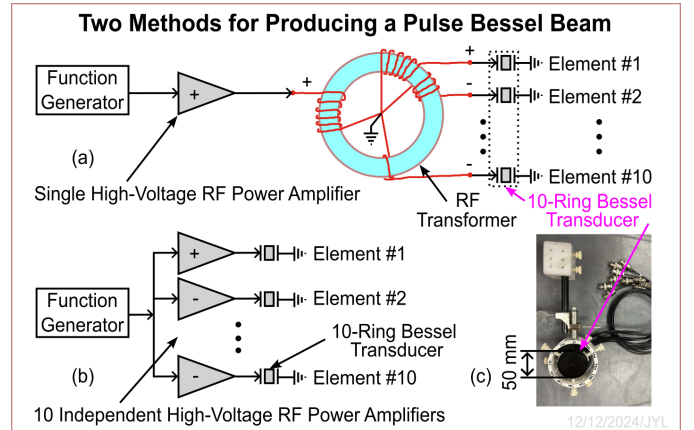


**Fig. 1.** Two methods to drive a 10-ring annular array transducer (Bessel transducer) to produce pulse Bessel beams. (a) Producing the Bessel beams with single high-voltage radio-frequency (RF) power amplifier in combination with an RF transformer. (b) Producing the Bessel beams with 10 independent high-voltage RF power amplifiers. (c) A photo of the 10-ring annular array transducer.

#### B. Depth of Field of Bessel Beam

As mentioned in Section II “Theoretical Preliminaries”, in theory, Bessel beams can maintain their transverse beam profiles of a narrow beamwidth as the waves propagate to an infinite distance. In practice, when Bessel beams are produced with a finite aperture, they have a very large depth of field [2]-[5]. The depth of field of a Bessel beam produced with a finite aperture is given by [2][8][54]:

$$DOF_B = \frac{D}{2} \sqrt{\left(\frac{k_0}{\alpha}\right)^2 - 1}, \quad (9)$$

where  $D$  is the diameter of the transducer. Given the parameters  $\alpha = 1202.45 \text{ m}^{-1}$ , center frequency  $f_0 = 2.5 \text{ MHz}$ , speed of sound in water  $c = 1500 \text{ m/s}$ , and  $D = 50 \text{ mm}$ , the calculated  $DOF_B = 216.28 \text{ mm}$  (about  $360.47 \lambda$ , where  $\lambda = c / f_0 = 0.6 \text{ mm}$  is the center wavelength). The full-width-at-half-maximum (FWHM) beamwidth of the Bessel beam is determined by the -6-dB width of the center lobe of the  $J_0(\alpha r)$  Bessel function, which is about  $2.53 \text{ mm}$  (or  $4.22 \lambda$ ) with the  $\alpha$  value above [5]. As a comparison, if the same annular array transducer is apodized to produce a Gaussian beam that has a 25-mm FWHM aperture at the surface of the transducer and is focused at  $z = 120 \text{ mm}$ , the depth of field will only be about  $24.4 \text{ mm}$  ( $41 \lambda$ ) [5]. As the FWHM aperture of the focused Gaussian beam is increased or the focal length is decreased (i.e., the  $f$ -number is reduced), the depth of field will be even smaller.

The large depth of field of the Bessel beams is beneficial to medical imaging [5][7][48]. If a single-element transducer focused at a fixed distance is used in imaging, it will have a

short depth of field as mentioned above and the image lateral resolution will decrease quickly outside of the depth of field, especially when the  $f$ -number is small, leading to a poor image quality. Although the focal distance of an annular array transducer can be changed, it is still fixed in each transmission. Thus, to form an image of an effectively large depth of field, a montage of images obtained from multiple transmissions focused at different distances is needed. The montage process is to cut a strip of the image around each focal distance and then piece it together with the strips obtained from other focal distances, which takes time and thus reduces image frame rate. Also, to focus a beam electronically with an annular array transducer, the electrical signals that drive the annular array transducer need to be delayed precisely, complicating the driving circuits. Thus, using Bessel beams can help to solve these problems.

### C. Production of Bessel Beams

The 10-ring annular array transducer above was driven by 10 independent high-voltage RF power amplifiers to produce Bessel beams. The output voltage of each RF power amplifier was proportional to the absolute value of the peak of the corresponding lobe of the  $J_0(\alpha r)$  Bessel function and the phase ( $0^\circ$  or  $180^\circ$ ) of the RF power amplifier was determined by the sign of the peak (see Fig. 1(b)). The maximum output voltage of the power amplifiers was set to about 90 Vp (peak voltage) and the transducer was driven by a one-cycle 2.5-MHz electrical sine signal. Because the 10 high-voltage RF power amplifiers used were bulky and consumed a lot of power (see Figs. 2(c) and 2(d)), it would be difficult to use them to produce Bessel beams for wearable medical ultrasound imaging [42]-[43] or wearable super-resolution imaging [44]-[46]. To reduce the size, weight, and power consumption, only one high-voltage RF power amplifier should be used. However, as mentioned above, single RF power amplifier can only drive a single-element transducer focused at a fixed distance, resulting in a short depth of field and poor image quality.

To address the issues of multiple high-voltage RF power amplifiers, a method that uses single RF power amplifier in combination with an RF transformer was developed to produce Bessel beams (see Fig. 1(a), Fig. 2(a), and Fig. 2(b)). The RF transformer consisted of one primary winding of 45 turns of a Gauge 22 (0.644 mm diameter) magnetic wire and 10 secondary windings of approximately 45.0, 18.1, 13.5, 11.2, 9.83, 8.84, 8.10, 7.52, 7.05, and 6.66 turns that were proportional to the absolute values of the peaks of the  $J_0(\alpha r)$  Bessel function, i.e., 1.00, -0.4028, 0.3001, -0.2497, 0.2184, -0.1965, 0.1801, -0.1672, 0.1567, and -0.1480, respectively, for Rings #1 to #10 of the annular array transducer. If the peak value of the Bessel function was negative, the direction of the corresponding winding was reversed, producing a  $180^\circ$  phase shift. The magnetic wires used in the secondary windings were Gauge 28 (0.321 mm diameter) for Ring #1 and Gauge 24 (0.511 mm diameter) for Rings #2 to #9 for simplicity. Since the enamel on the magnetic wires can withstand at least 20 V/ $\mu\text{m}$  and the thickness of the enamel is usually more than 30  $\mu\text{m}$ , these magnetic wires are safe to be used for a peak

voltage of about 90 Vp (or 180 Vpp peak to peak) without additional insulations. The core of the transformer used had a toroidal shape and was made of Cobalt-Nickle-Zinc (CoNiZn) (11-780-K, Ferronics, Bethlehem, PA, USA). The outer (O.D.) and inner (I.D.) diameters of the toroidal core were 22.10 mm and 13.72 mm, respectively, and the height of the core was  $h = 6.35$  mm. The self-inductance of a winding of toroid can be calculated with (see Eq. 7.28 in Ref. [56] at P.325):

$$L = \frac{\mu_0 \mu_r M^2 h}{2\pi} \ln\left(\frac{\text{O.D.}}{\text{I.D.}}\right), \quad (10)$$

where  $\mu_0 = 4\pi \times 10^{-7}$  H/m is the permeability constant in vacuum,  $\mu_r = 125$  is the relative permeability of the toroidal core, and  $M$  is the number of turns. With  $M = 45$  for the primary winding, the calculated self inductance was about 153.3  $\mu\text{H}$  or an impedance of 2407.3 ohms at 2.5 MHz.

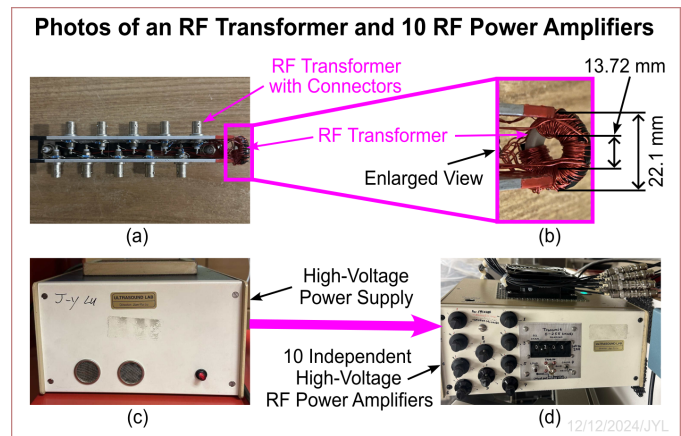


**Fig. 2.** Photos of the high-voltage RF power amplifiers and the RF transformer to drive the 10-ring annular array transducer to produce pulse Bessel beams. (a) The RF transformer and its Bayonet Neill-Concelman (BNC) connectors for the 10-ring annular array transducer. (b) Enlarged view of the RF transformer. (c) High-voltage DC power supply. (d) 10 independent high-voltage RF power amplifiers to drive the 10-ring annular array transducer.

### D. Experiment System

Fig. 3 shows an experiment system for measuring pulse Bessel beams produced by the 10-ring annular transducer (see Fig. 1(c)). In the experiments, the annular array transducer and a broadband (1-20 MHz) polyvinylidene fluoride (PVDF) needle hydrophone (TNU001A, NTT Systems, Inc., Seattle, Washington, USA) of 0.6-mm diameter were placed in a water tank as shown on the right and left hand sides of Fig. 3(a) respectively. A block diagram of the experiment system is given in Fig. 3(b). During the experiments, a step motor moved (scanned) the annular array transducer along the  $x$  axis over a distance of 50 mm in 200 equal-distance steps (the step size was 0.25 mm) (since the motion between the hydrophone and the annular array transducer is relative, the hydrophone can be scanned instead). Since the Bessel beams were axially symmetric, only one scan across the axial axis of the annular array transducer was necessary to obtain entire pulse Bessel beams at an axial distance,  $z$ . At each scanning step, an unsynchronized trigger signal was generated by the

motor unit and then sent to a digitizing unit to produce another trigger signal synchronized to the clock of the digitizer. The synchronized trigger was sent to a function generator (HP8116A, Hewlett-Packard Company, CA, USA) to produce a 1-cycle and 2.5-MHz electrical sine signal that was sent to either 10 home-made independent high-voltage RF power amplifiers (see Fig. 1(b) and Figs. 2(c) and 2(d)) to drive the 10-ring annular array transducer or a commercial RF power amplifier (ENI2100L, Electronics and Innovation, Ltd., NY, USA) to drive the RF transformer (see Fig. 1(a), Figs. 2(a), and Fig. 2(b)) that was connected to the 10-ring annular array transducer. The ultrasound pulse Bessel beams produced in water were received by the PVDF needle hydrophone and the received signals were amplified, filtered by a 0.5-7.5 MHz band-pass filter, digitized at 50 MS/s sampling rate and 12-bit resolution, and then stored on a hard disk.

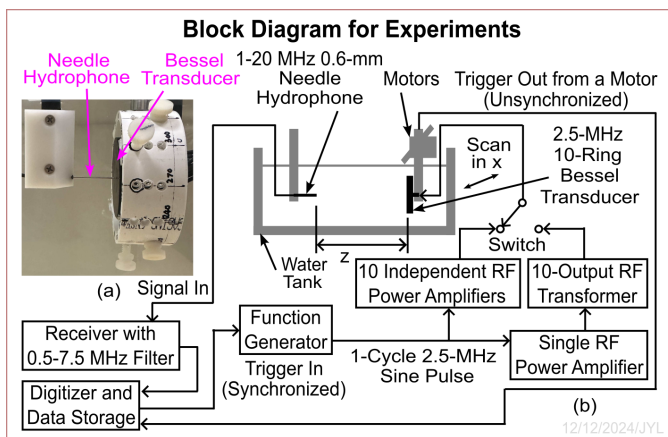


**Fig. 3.** Block diagram of the experiments. (a) A photo of the needle hydrophone and the 10-ring annular array transducer (Bessel transducer). (b) Block diagram of the experiments. The 10-ring annular array transducer was placed on the right hand side of the water tank. Pulse Bessel beams produced by the transducer was received by a broadband PVDF needle hydrophone (0.6-mm in diameter and 1-20 MHz bandwidth, see the left hand side of the water tank). To map the Bessel beams, the transducer was moved (scanned) along the  $x$  axis in multiple equal-distance steps and the tip of the needle hydrophone acrossed the axis of the transducer. At each step, an unsynchronized trigger signal was produced from the motor unit and sent to the digitizer unit that produced another trigger signal synchronized to the clock of the digitizer. The synchronized trigger was used to trigger a function generator to produce a 1-cycle and 2.5-MHz electrical sine signal that was amplified to drive the transducer to produce pulse Bessel beams. The Bessel beams were measured by the hydrophone to produce electrical signals that were amplified, filtered, digitized, and then stored in a hard disk. The switch indicates that the transducer can be driven either by single high-voltage RF power amplifier in combination with an RF transformer or by 10 independent high-voltage RF power amplifiers.

#### IV. RESULTS

Fig. 4 shows an analytic envelope of the RF pulse Bessel beams measured by the 0.6-mm broadband PVDF needle hydrophone at 3 axis distances,  $z = 1$  mm (Figs. 4(a) and 4(d)), 100 mm (Figs. 4(b) and 4(e)), and 200 mm (Figs. 4(c) and 4(f)) from the surface of the annular array transducer using the experiment system in Fig. 3. Figs. 4(a) to 4(c) were obtained using the single high-voltage RF power amplifier in

combination with the RF transformer above to drive the 10-ring annular array transducer. Figs. 4(d) to 4(f) are the same as Figs. 4(a) to 4(c) respectively, except that they were obtained with the 10 independent high-voltage RF power amplifiers (see Fig. 1(b), Fig. 2(c), and Fig. 2(d)). In each panel of Fig. 4, the vertical and horizontal dimensions represent the scanning distance (50 mm) of the annular array transducer in the water tank and the time (10.24  $\mu$ s) respectively. The color bar on the right hand side of Fig. 4 represents a normalized magnitude of the measured acoustic pressure in water. As mentioned before, the scaling parameter, the center frequency, and the speed of sound for the pulse Bessel beams were  $\alpha = 1202.45 \text{ m}^{-1}$ ,  $f_0 = 2.5 \text{ MHz}$ , and  $c = 1500 \text{ m/s}$  (or the center wavelength  $\lambda = 0.6 \text{ mm}$ ), respectively. It is clear from Fig. 4 that the pulse Bessel beams have a narrow FWHM mainlobe beamwidth (close to the theoretical value of 2.53 mm or  $4.22 \lambda$ ) and stay in focus from the surface of the transducer to over  $z = 200$  mm (the depth of field calculated from Eq. (9) was about 216.28 mm or  $230.47 \lambda$ ). Compare Figs. 4(a) to 4(c) with Figs. 4(d) to 4(f) respectively, they are similar. This means that the pulse Bessel beams can be produced well with the method that uses single high-voltage RF power amplifier in combination with an RF transformer, which will greatly reduce the power consumption, size, and weight of the driving circuits and make it easier to use the Bessel beams in wearable applications such as wearable medical ultrasound imaging [42]-[43] and wearable super-resolution imaging [44]-[46]. Also as mentioned in Section II “Theoretical Preliminary”, unlike the X waves [32][54][55], the pulse length (or the axial resolution in a pulse-echo imaging) of the pulse Bessel beams changes with propagation distances due to dispersion.

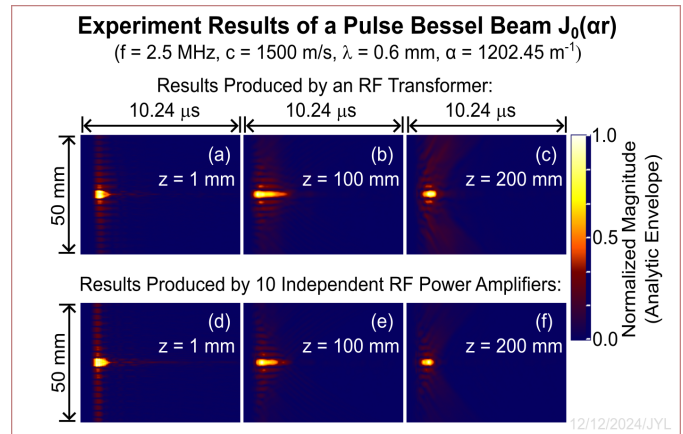


**Fig. 4.** Measured pulse Bessel beams at different axial distances using single high-voltage RF power amplifier in combination with an RF transformer (top row) and using 10 independent high-voltage RF power amplifiers (bottom row) to drive a 10-ring annular array transducer. (a) and (d) Pulse Bessel beams measured at axial distance  $z = 1$  mm from the surface of the transducer. (b) and (e) are the same as (a) and (d) respectively except that they were obtained at  $z = 100$  mm. (c) and (f) also are the same as (a) and (d) respectively except that they were obtained at  $z = 200$  mm. The pulse Bessel beams were produced by driving an annular array transducer with a 1-cycle electrical sine signal and were measured by scanning the annular array transducer along the  $x$  axis for 50 mm. The signals were received by a 0.6-mm broadband PVDF needle hydrophone and were digitized at 50 ms/s sampling rate and 12-bit resolution for 10.24  $\mu$ s. The analytic envelope of the pulse

Bessel beams was displayed and the color bar on the right indicates normalized magnitude.

Fig. 5 shows line plots of the pulse Bessel beams in Fig. 4 at three axial distances  $z = 1$  mm (Fig. 5(a)), 100 mm (Fig. 5(b)), and 200 mm (Fig. 5(c)) from the surface of the annular array transducer. The solid lines (black) were the results obtained with the single high-voltage RF power amplifier in combination with the RF transformer and the dotted lines (pink) were those obtained with the 10 independent high-voltage RF power amplifiers. The horizontal and vertical axes represent respectively the scanning positions and the maximum value along each horizontal line of the panels in Fig. 4. Each plot was normalized to its maximum in the vertical axis and shows the sidelobes of a pulse Bessel beam. From the plots in Fig. 5, it is clear that the pulse Bessel beams produced with and without using multiple RF power amplifiers were very close.

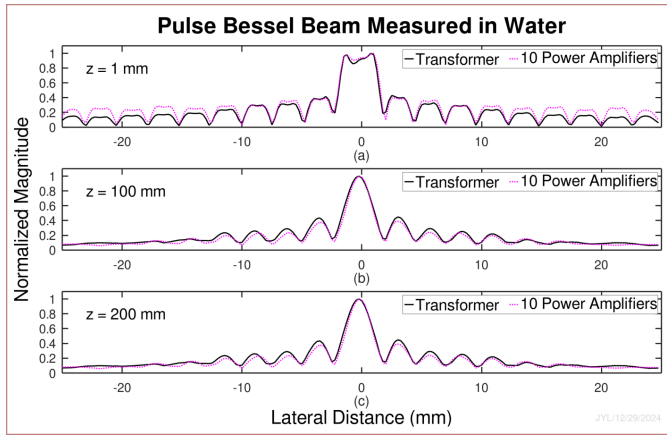


**Fig. 5.** Line plots of the pulse Bessel beams measured across the axial axis of the annular array transducer along the  $x$  axis (lateral distance) at (a)  $z = 1$  mm, (b)  $z = 100$  mm, and (c)  $z = 200$  mm. The solid (black) and dotted (pink) lines correspond to the top (using single high-voltage RF power amplifier in combination with an RF transformer) and bottom (using 10 independent high-voltage RF power amplifiers) rows of Fig. 4 respectively. The vertical and horizontal axes represent the normalized magnitude of the pulse Bessel beams and the lateral distance along the  $x$  axis (parallel to the transducer surface) respectively. The line plots were normalized to their respective maxima, and they were obtained by taking the maximum value from each row of the panels in Figs. 4(a) to 4(f), which shows the maximum sidelobes of the pulse Bessel beams.

## V. DISCUSSION

### A. Optimizing for Wearable Applications

From both Figs. 4 and 5, it is clear that almost identical pulse Bessel beams can be produced by either single high-voltage RF power amplifier in combination with an RF transformer (see Fig. 1(a), Fig. 2(a), and Fig. 2(b)) or 10 independent high-voltage RF power amplifiers (see Fig. 1(b), Fig. 2(c), and Fig. 2(d)) to drive a 10-ring annular array transducer (see Fig. 1(c)). However, for wearable applications such as wearable medical ultrasound imaging [42]-[43] or wearable super-resolution imaging [44]-[46], the method that uses single RF power amplifier in combination with an RF transformer to produce the pulse Bessel beams is preferred

due to reduced power, size, and weight as compared to that using multiple RF power amplifiers. To further reduce the size and weight, both the RF transformer and the annular array transducer in Fig. 1(c), Fig. 2(a), and Fig. 2(b) can be optimized. For example, the size of the ferrite core can be reduced if the average power is lower (such as a lower pulse duty cycle), and the diameter of the magnetic wires can be decreased if the actual maximum current is smaller. The diameter of the annular array transducer also can be reduced, and the frequency (or penetration depth) and the image lateral resolution can be optimized according to Eq. (9) for a specific application.

### B. Lateral Beamwidth or Image Lateral Resolution

A small lateral beamwidth means a higher lateral resolution when Bessel beams are used in imaging (see Fig. 6(a)). The FWHM lateral beamwidth of a Bessel beam is determined by the FWHM width of the mainlobe of the  $|J_0(\alpha r)|$  Bessel function and thus is inversely proportional to the scaling parameter  $\alpha$ . Eq. (9) gives a relationship among the depth of field of a Bessel beam, the scaling parameter  $\alpha$ , the diameter of the annular array transducer  $D$ , and the center frequency  $f_0$ . As an example, the following 10-ring annular array transducer could be used to produce a pulse Bessel beam for a wearable imaging application:  $D = 25$  mm,  $f_0 = 5$  MHz,  $\alpha = 2404.90$   $\text{m}^{-1}$  (lateral beamwidth of about 1.26 mm), and a depth of field (or penetration depth) of about 108.14 mm. Notice that the lateral beamwidth will be smaller if the Bessel beam is used in both transmit and receive in the imaging system of Fig. 6(a).

### C. Dispersion and Image Axial Resolution

It is seen from Fig. 4 that the pulse length of the Bessel beams changes with the axial distance  $z$  (a longer pulse length means a lower axial resolution in a pulse-echo imaging (see Fig. 6(a)). The elongation of the pulse length during the wave propagation was caused by the dispersion of the Bessel beams (i.e., the speed of the wave,  $c_1 = \omega_0 / \beta$ , changes with the frequency in the propagation term  $e^{i(\beta z - \omega_0 t)} = e^{i\beta(z - c_1 t)}$  of Eq. (7) or Eq. (8)). To avoid the dispersion, X waves that have a constant speed  $c_1 = c / \cos(\zeta) \geq c$  could be used [32][54]-[55], where  $\zeta$  is the Axicon angle [38][52] and  $c_1$  is both the phase and group velocities of the waves (since  $c_1 \geq c$ , X waves are superluminal in optics and supersonic in ultrasound). However, X waves are more complicated to produce than Bessel beams.

### D. Sidelobes

The sidelobes of the pulse Bessel beams are relatively high (see Figs. 4 and 5) and decrease in proportional to  $1/\sqrt{r}$  (where  $r$  is the radial distance), which is the asymptotic behavior of the Bessel function. For comparison, the sidelobes of a conventional focused beam at its focal distance is proportional to  $1/(\sqrt{r})^3$ . Sidelobes reduce image contrast and should be minimized. In the pulse-echo imaging system in

Fig. 6(a), the sidelobes is reduced (i.e., proportional to  $1/r$ ).

### E. Depth of Field

The depth of field of the pulse Bessel beams in Figs. 4 and 5 are very large (about 216.28 mm with a small lateral beamwidth of about 2.53 mm) (see Eq. (9) and the Bessel pulse-echo imaging system in Fig. 6(a)). As a comparison, the single-element focused transducer in the pulse-echo imaging system of Fig. 6(b) has a very short depth of field, despite both imaging systems in Figs. 6(a) and 6(b) using the same single high-voltage RF power amplifier and thus having a similar size and weight.

### F. Self Healing

Both Bessel beams and X waves as well as other beams such as Airy beams have demonstrated a strong self-healing ability [6][51] due to their relatively high sidelobes. When one part of the beam is obstructed, the remaining energy in the sidelobes will reconstruct the beam after the obstacle. This can also be seen in Fig. 5: despite the two pulse Bessel beams obtained at  $z = 1$  mm with (solid line) and without (dotted line) using the RF transformer had different sidelobes (see Fig. 5(a)) due to an integer rounding of the number of turns of the secondary windings of the RF transformer and the errors of setting the gains of the 10 RF power amplifiers, their sidelobes were almost the same at  $z = 100$  mm and 200 mm (see Figs. 5(b) and 5(c)). I.e., the disturbance of the pulse Bessel beams at  $z = 1$  mm did not have much an effect after some distance from the disturbance. Self healing will reduce the shadows cast behind objects such as hard tumors in medical ultrasound imaging [51].

### G. Impedance Matching

The pulse lengths of the pulse Bessel beams in Fig. 4 are different with the two methods (see the top and bottom rows of Fig. 4) at each axial distance,  $z$ . This is because there was no electrical impedance matching (tuning) between the driving circuits and the 10-ring annular array transducer in the experiments. With a proper electrical impedance matching, it is expected that the bandwidth of the transducer will be increased and the pulse length will be shortened, which will increase the axial resolution in a pulse-echo imaging. Also, increasing the bandwidth of the RF transformer will reduce the pulse lengths if the dispersion is small (if  $\alpha$  is much smaller than  $k_0$ , the dispersion can be ignored, see Eq. (6)).

### H. Bessel Imaging System Using an RF Transformer

An example of a pulse-echo imaging system using a Bessel beam in both transmit and receive is shown in Fig. 6(a), where the Bessel beam is produced by single high-voltage RF power amplifier, an RF transformer, and an  $N$ -ring annular array transducer, where  $N$  is an integer. After a pulse Bessel beam is transmitted, echoes from the object to be imaged are received by the same transducer to produce the same Bessel response (reciprocal) to form an RF A-line using a circuit that sums the weighted electrical signals (using preamplifiers of different gains and polarities) from the rings of the annular array transducer via transmit/receive (T/R) switches (see Fig.

6(a)). The annular array transducer can be scanned by a wobbler [47]-[48] or moving reflectors [49]-[50] to obtain multiple A-lines to form either 2D or three-dimensional (3D) images. The RF A-lines can be sent wirelessly to a remote device to display images, or, be processed to display images locally using a low-power device such as liquid crystal display (LCD). To reduce the sidelobes of the pulse-echo imaging system in Fig. 6(a), instead of using the Bessel beam in receive, a dynamically focused Gaussian beam can be used at the expenses of needing additional circuit components for dynamic time delays. The pulse-echo imaging system in Fig. 6(a) is compared to the simplest conventional pulse-echo imaging system that uses a single-element transducer focused at a fixed distance (see Fig. 6(b)). It is seen that both imaging systems use the same single high-voltage RF power amplifier and thus have a similar power consumption, size, and weight. However, the imaging system in Fig. 6(b) has a much shorter depth of field and thus poorer image quality.

### I. Super-Resolution Imaging

Recently, a PSF-modulation super-resolution imaging method was developed [44]-[46]. In a computer simulation (see Figs. 8 and 9 in Ref. [44]), it shows that super-resolution images can be reconstructed using a phase modulation (the phase modulation can be introduced by a shear wave produced by a focused annular array transducer that produces a focused Bessel beam [5][15]). Also, the method can be used for remote super-resolution mapping of a pulse Bessel beam (see experiment results in Figs. 6 and 7 in Ref. [46]). In addition, since the method increases image resolution by introducing high spatial frequencies through modulating the point-spread function (PSF) of a linear shift-invariant (LSI) system and many imaging systems can be described or approximately described as an LSI system, in principle, the method can be applied not only to the wave-based imaging systems such as ultrasound, optical, electromagnetic, radar, and sonar; but also to other imaging systems such as X-ray radiography, X-ray CT, magnetic resonance imaging (MRI), gamma camera, single-photon emission computerized tomography (SPECT), and positron emission tomography (PET) to achieve super resolution or high resolution [45].

Therefore, the PSF-modulation super-resolution imaging method can work directly with either the Bessel or the conventional imaging system in Figs. 6 using either a physical or non-physical modulator [44]. Alternatively, the Bessel beam produced with the RF transformer in Fig. 1(a) can be used to remotely generate a modulator for wearable super-resolution ultrasound imaging to monitor diseased tissues such as tumors deep in the body as follows: First, focus the Bessel beam generated with the RF transformer in Fig. 1(a) by attaching a physical lens of a desired focal length to produce a ring of radiation force that creates a ring of shear wave inside a tumor to be monitored deep in the body [15] (also see Fig. 9 in Ref. [44]). The shear wave will then focus to a feature of about a half of the shear-wave wavelength at the center of the ring (the shear-wave wavelength can be small due to its low speed in biological soft tissues). Second, add a second set of the secondary windings that do not have alternating polarities to the RF transformer in Fig. 1(a) to produce a conventional

focused beam. Third, add electronic switches to the annular array transducer to select either the first or the second set of the secondary windings to produce either a focused Bessel beam or a conventional focused beam. Fourth, modulate the conventional focused beam with the focused shear wave that causes a phase shift and introduces high spatial frequency components. Echoes returned will be focused (or dynamically focused) to form an A-line (the phase shift due to the shear wave can be detected by subtracting the A-lines obtained with and without the shear wave) (see Figs. 8 and 9 in Ref. [44]). Finally, scan the focused Bessel beam together with the conventional focused beam to obtain multiple A-lines to reconstruct a super-resolution image of the tumor around the focal distance deep in the body [47]-[50].

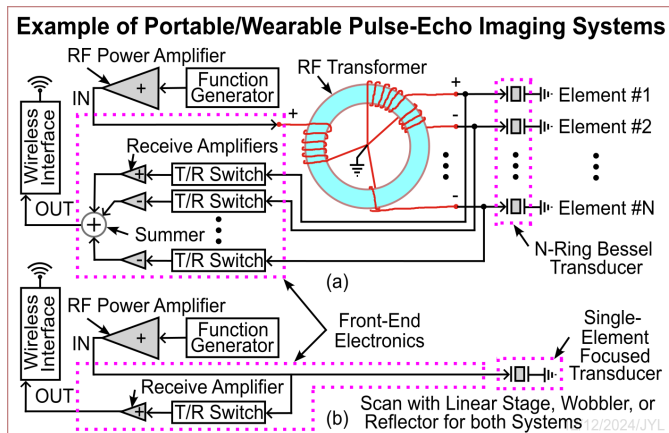


**Fig. 6.** An example of pulse-echo imaging systems using a pulse Bessel beam and a conventional focused beam. (a) Imaging system that uses single high-voltage RF power amplifier in combination with an RF transformer to produce a pulse Bessel beam of a large depth of field. The received signals obtained via T/R switches are combined to produce a Bessel beam response or a conventional dynamically focused Gaussian beam to reduce sidelobes. The combined signal can then be transmitted wirelessly to a remote device for image display or be processed for image display on a local device. Images can be formed by scanning the beams with a wobbler [47]-[48] or moving reflectors [49]-[50]. (b) The simplest imaging system that uses the same single high-voltage RF power amplifier and a single-element transducer focused at a fixed distance for comparison with (a). Notice that although both imaging systems have a similar power consumption, size, and weight, the imaging system in (b) has a much shorter depth of field and poorer image quality.

## VI. CONCLUSION

A method that uses single high-voltage RF power amplifier in combination with an RF transformer was developed to produce pulse Bessel beams that have a large depth of field [5]. This method simplifies the electronics used to drive the annular array transducer and reduces their power, size, and weight, making it easier to apply the Bessel beams to wearable medical ultrasound imaging [42]-[43] or wearable super-resolution imaging [44]-[46]. Experiments were performed with a 10-ring, 50-mm diameter, 2.5-MHz center frequency, and broadband (about 72% -6dB relative one-way bandwidth) annular array transducer. The RF transformer was custom made and was consisted of one primary and 10 secondary windings. The results show that pulse Bessel beams of a small

beamwidth of about 2.53 mm (4.22 wavelengths) and a large depth of field of about 216 mm (about 360 wavelengths) can be produced with the new method.

## ACKNOWLEDGMENT

The author would like to thank Dr. Pengfei Song of the Duke University for a discussion on a potential of the method developed in this paper to wearable applications.

## REFERENCES

- [1] J. A. Stratton, *Electromagnetic Theory*. New York and London: McGraw-Hill Book Company, 1941, Page 356.
- [2] Durnin, J. "Exact solutions for nondiffracting beams. I. The scalar theory." *JOSA A* 4, no. 4 (1987): 651-654.
- [3] J. Durnin, J. J. Miceli Jr, and J. H. Eberly. "Diffraction-free beams." *Physical review letters* 58, no. 15 (1987): 1499.
- [4] J. Durnin, J. J. Miceli Jr, and J. H. Eberly. "Experiments with nondiffracting needle beams." In *International Quantum Electronics Conference*, p. FHH5. Optica Publishing Group, 1987.
- [5] Jian-yu Lu and J. F. Greenleaf, "Ultrasonic nondiffracting transducer for medical imaging," *IEEE Transactions on Ultrasonics, Ferroelectrics, and Frequency Control*, vol. 37, no. 5, pp. 438-447, September 1990.
- [6] X. Chu. "Analytical study on the self-healing property of Bessel beam." *The European Physical Journal D* 66 (2012): 1-5.
- [7] Jian-yu Lu and J. F. Greenleaf, "Pulse-echo imaging using a nondiffracting beam transducer," *Ultrasound in Medicine and Biology*, vol. 17, no. 3, pp. 265-281, May 1991.
- [8] Jian-yu Lu, H. Zou, and J. F. Greenleaf, "Biomedical ultrasound beam forming," *Ultrasound in Medicine and Biology*, vol. 20, no. 5, pp. 403-428, July 1994.
- [9] Jian-yu Lu, J. Cheng, and B. C. Cameron, "Low sidelobe limited diffraction optical coherence tomography," in *Coherence Domain Optical Methods in Biomedical Science and Clinical Applications VI*, Valery V. Tuchin, Joseph A. Izatt, James G. Fujimoto, Editors, *Proceedings of SPIE*, vol. 4619, pp. 300-311, 2002.
- [10] N. Wang and J. Yao. "Sound Out the Deep Clarity: Super-resolution Photoacoustic Imaging at Depths." *IEEE Transactions on Ultrasonics, Ferroelectrics, and Frequency Control* (2024).
- [11] Jian-yu Lu, X.-L. Xu, H. Zou, and J. F. Greenleaf, "Application of Bessel beam for Doppler velocity estimation," *IEEE Transactions on Ultrasonics, Ferroelectrics, and Frequency Control*, vol. 42, no. 4, pp. 649-662, July 1995.
- [12] Jian-yu Lu and J. F. Greenleaf, "Diffraction-limited beams and their applications for ultrasonic imaging and tissue characterization," in *New Developments in Ultrasonic Transducers and Transducer Systems*, F. L. Lizzi, Editor, *Proceedings of SPIE*, vol. 1733, pp. 92-119, 1992.
- [13] Jian-yu Lu and J. F. Greenleaf, "Producing deep depth of field and depth-independent resolution in NDE with limited diffraction beams," *Ultrasonic Imaging*, vol. 15, no. 2, pp. 134-149, April 1993.
- [14] Jian-yu Lu, "Designing limited diffraction beams," *IEEE Transactions on Ultrasonics, Ferroelectrics, and Frequency Control*, vol. 44, no. 1, pp. 181-193, January 1997.
- [15] Jian-yu Lu, "Focused limited-diffraction beams for ultrasound therapy applications," in *2021 IEEE International Ultrasonics Symposium Proceedings*, pp.1-4, 2021.
- [16] F. G. Mitri. "Single Bessel tractor-beam tweezers." *Wave Motion* 51, no. 6 (2014): 986-993.
- [17] T. A. Moura, U. M. S. Andrade, J. B. S. Mendes, and M. S. Rocha. "Modulating the trapping and manipulation of semiconductor particles using Bessel beam optical tweezers." *Optics and Lasers in Engineering* 170 (2023): 107778.
- [18] S. Jiménez-Gambín, N. Jiménez, J. M. Benlloch, and F. Camarena. "Generating Bessel beams with broad depth-of-field by using phase-only acoustic holograms." *Scientific reports* 9, no. 1 (2019): 20104.
- [19] S. Lin, Li Gong and Z. Huang. "Super - Resolution Two - Photon Fluorescence Tomography Through the Phase - Shifted Optical

- Beatings of Bessel Beams for High - Resolution Deeper Tissue 3D Imaging." *Laser & Photonics Reviews* 18, no. 2 (2024): 2300634.
- [20] T. Meinert and A. Rohrbach. "Light-sheet microscopy with length-adaptive Bessel beams." *Biomedical optics express* 10, no. 2 (2019): 670-681.
- [21] H. Kim, K. Mishchik, A. Voronov, J. Kim, W. Jung, J. You, S. Jang, S. Park, K. Yoo, S. Baek, J. Ryu, S. Jeong, C. Roh. "Optimization of Bessel beam optics for high-quality glass cutting." In *Laser-based Micro-and Nanoprocessing XVI*, vol. 11989, pp. 6-17. SPIE, 2022.
- [22] Z. Lu, Z. Guo, M. Fan, M. Guo, C. Li, Y. Yao, H. Zhang, W. Lin, H. Liu, and B. Liu. "Tunable bessel beam shaping for robust atmospheric optical communication." *Journal of Lightwave Technology* 40, no. 15 (2022): 5097-5106.
- [23] D. Y. Vasylyev, A. A. Semenov, and W. Vogel. "Toward global quantum communication: beam wandering preserves nonclassicality." *Physical review letters* 108, no. 22 (2012): 220501.
- [24] M. McLaren, M. Agnew, J. Leach, F. S. Roux, M. J. Padgett, R. W. Boyd, and A. Forbes. "Entangled bessel-gaussian beams." *Optics express* 20, no. 21 (2012): 23589-23597.
- [25] M. McLaren, T. Mhlanga, M. J. Padgett, F. S. Roux, and A. Forbes. "Self-healing of quantum entanglement after an obstruction." *Nature communications* 5, no. 1 (2014): 3248.
- [26] L. Schächter and W. D. Kimura. "Electron beam guiding by a laser Bessel beam." *Physical Review Accelerators and Beams* 23, no. 8 (2020): 081301.
- [27] B. Hafizi, E. Esarey, and P. Sprangle. "Laser-driven acceleration with Bessel beams." *Physical Review E* 55, no. 3 (1997): 3539.
- [28] D. Mugnai and P. Spalla. "Electromagnetic propagation of Bessel-like localized waves in the presence of absorbing media." *Optics communications* 282, no. 24 (2009): 4668-4671.
- [29] O. Brzobohatý, T. Čížmár, and P. Zemánek. "High quality quasi-Bessel beam generated by round-tip axicon." *Optics express* 16, no. 17 (2008): 12688-12700.
- [30] M. A. Mahmoud, M. Y. Shalaby, and D. Khalil. "Propagation of Bessel beams generated using finite-width Durnin ring." *Applied optics* 52, no. 2 (2013): 256-263.
- [31] N. Jiménez, R. Picó, V. Sánchez-Morcillo, V. Romero-García, L. M. García-Raffi, and K. Staliunas. "Formation of high-order acoustic Bessel beams by spiral diffraction gratings." *Physical Review E* 94, no. 5 (2016): 053004.
- [32] Jian-yu Lu and J. F. Greenleaf, "Nondiffracting X waves --- exact solutions to free-space scalar wave equation and their finite aperture realizations," *IEEE Transactions on Ultrasonics, Ferroelectrics, and Frequency Control*, vol. 39, no. 1, pp. 19-31, January 1992.
- [33] N. Chattopadhyay, E. A. Rogers, D. Cofield, W. T. Hill III, and R. Roy. "Generation of nondiffracting Bessel beams by use of a spatial light modulator." *Optics letters* 28, no. 22 (2003): 2183-2185.
- [34] Q. Zhang, X. M. Cheng, H. W. Chen, B. He, Z. Y. Ren, Y. Zhang, and J. T. Bai. "Diffraction-free, self-reconstructing Bessel beam generation using thermal nonlinear optical effect." *Applied Physics Letters* 111, no. 16 (2017).
- [35] P. Steinvurzel, K. Tantiwanichapan, M. Goto, and S. Ramachandran. "Fiber-based Bessel beams with controllable diffraction-resistant distance." *Optics letters* 36, no. 23 (2011): 4671-4673.
- [36] J. A. Campbell and S. Soloway. "Generation of a nondiffracting beam with frequency - independent beamwidth." *The Journal of the Acoustical Society of America* 88, no. 5 (1990): 2467-2477.
- [37] D. K. Hsu, F. J. Margetan, and D. O. Thompson. "Bessel beam ultrasonic transducer: Fabrication method and experimental results." *Applied physics letters* 55, no. 20 (1989): 2066-2068.
- [38] C. B. Burckhardt, H. Hoffmann, and P-A. Grandchamp. "Ultrasound axicon: a device for focusing over a large depth." *The Journal of the Acoustical Society of America* 54, no. 6 (1973): 1628-1630.
- [39] M. Moshfeghi. "Sidelobe suppression in annular array and axicon imaging systems." *The Journal of the Acoustical Society of America* 83, no. 6 (1988): 2202-2209.
- [40] Y. Zhao, H. Y. Dong, S. Zhao, S. Min, J. Cheng, B. Li, F. Chi, and S. Liu. "Design of broadband impedance-matching Bessel lens with acoustic metamaterials." *Journal of Applied Physics* 126, no. 6 (2019).
- [41] Jian-yu Lu and J. F. Greenleaf, "A study of two-dimensional array transducers for limited diffraction beams," *IEEE Transactions on Ultrasonics, Ferroelectrics, and Frequency Control*, vol. 41, no. 5, pp. 724-739, September 1994.
- [42] H. Huang, R. S. Wu, M. Lin, and S. Xu. "Emerging wearable ultrasound technology." *IEEE Transactions on Ultrasonics, Ferroelectrics, and Frequency Control* 71, no. 7 (2023): 713-729.
- [43] H. Hu, H. Huang, M. Li, X. Gao, L. Yin, R. Qi, R. S. Wu, X. Chen, Y. Ma1, K. Shi, C. Li, T. M. Maus, B. Huang, C. Lu, M. Lin, S. Zhou, Z. Lou, Y. Gu, Y. Chen, Y. Lei, X. Wang, R. Wang, W. Yue, X. Yang, Y. Bian, J. Mu, G. Park, S. Xiang, S. Cai, P. W. Corey, J. Wang, and S. Xu. "A wearable cardiac ultrasound imager." *Nature* 613, no. 7945 (2023): 667-675.
- [44] Jian-yu Lu, "Modulation of Point Spread Function for Super-Resolution Imaging." *IEEE Transactions on Ultrasonics, Ferroelectrics, and Frequency Control*, vol. 71, no. 1, pp. 153-177, January 2024.
- [45] Jian-yu Lu, "A general method to obtain clearer images at a higher resolution than theoretical limit," 186th Meeting of Acoustical Society of America, Acoustical Lay Language Paper, April 22, 2024 (<https://acoustics.org/a-general-method-to-obtain-clearer-images-at-a-higher-resolution-than-theoretical-limit/>).
- [46] Jian-yu Lu, "Remote Super-Resolution Mapping of Wave Fields," *IEEE Transactions on Ultrasonics, Ferroelectrics, and Frequency Control*, vol. 72, no. 3, pp. 370-379, March 2025.
- [47] B. S. Verma. "Ultrasound Transducers and Image Quality." *IETE Technical Review* 9, no. 2 (1992): 128-133.
- [48] Jian-yu Lu, T.-K. Song, R. R. Kinnick, and J. F. Greenleaf. "In vitro and in vivo real-time imaging with ultrasonic limited diffraction beams." *IEEE transactions on medical imaging* 12, no. 4 (1993): 819-829.
- [49] Z. Dong, S. Li, M. R. Lowerison, J. Pan, J. Zou, and P. Song. "Fast acoustic steering via tilting electromechanical reflectors (FASTER): A novel method for high volume rate 3-D ultrasound imaging." *IEEE transactions on ultrasonics, ferroelectrics, and frequency control* 68, no. 3 (2021): 675-687.
- [50] Z. Dong, S. Li, X. Duan, M. R. Lowerison, C. Huang, Q. You, S. Chen, J. Zou, and P. Song. "High-Volume-Rate 3-D Ultrasound Imaging Using Fast-Tilting and Redirecting Reflectors." *IEEE transactions on ultrasonics, ferroelectrics, and frequency control* 70, no. 8 (2023): 799-809.
- [51] X. Chen, F. Dong, C. Yin, J. Tu, D. Zhang, and X. Guo. "Ultrasonic imaging based on pulsed Airy beams." *IEEE Transactions on Ultrasonics, Ferroelectrics, and Frequency Control* 70, no. 9 (2023): 1146-1156.
- [52] F. S. Foster, M. S. Patterson, M. Arditi, and J. W. Hunt. "The conical scanner: a two transducer ultrasound scatter imaging technique." *Ultrasonic imaging* 3, no. 1 (1981): 62-82.
- [53] S. C. Gupta, "Delta function." *IEEE Transactions on Education* 1 (1964): 16-22.
- [54] Jian-yu Lu. Multi-Channel Data Transmission with X Wave and Bessel Pulses. *TechRxiv*. March 02, 2023. (DOI: <https://doi.org/10.36227/techrxiv.22083719.v2>).
- [55] Jian-yu Lu. "Limited-Diffraction Beams for Secure Fast Data Communications." In *2023 IEEE International Ultrasonics Symposium (IUS)*, pp. 1-4. IEEE, 2023.
- [56] D. J. Griffiths. *Introduction to electrodynamics*. Cambridge University Press, 2023.



**Jian-yu Lu** (S'86--M'88--SM'99--F'08--LF'25) received the B.S. degree in physics/electrical engineering from Fudan University, Shanghai, China, in February 1982; the M.S. degree in physics/acoustics from Tongji University, Shanghai, China, in 1985; and the Ph.D. degree in biomedical engineering from Southeast University, Nanjing, China, in 1988.

From December 1988 to February 1990, he was a Postdoctoral Research Fellow with the Mayo Medical School, Rochester, Minnesota, USA. Later, he was an Associate Professor of biophysics with the

Mayo Medical School and an Associate Consultant with the Department of Physiology and Biophysics, Mayo Clinic/Foundation, Rochester, Minnesota, USA. Since 1997, he has been a full Professor with the Department of Bioengineering, The University of Toledo (UT), Toledo, OH, USA, where he also has been an Adjunct Professor with the College of Medicine and Life Sciences, since 1998. His research interests are in acoustic imaging, devices, tissue identification; medical ultrasonic transducers; ultrasonic beam forming; and wave propagation physics.

Dr. Lu is a Life Fellow of IEEE (conferred in 2008), a Fellow of the American Institute of Ultrasound in Medicine (AIUM) (conferred in 2005), and a Fellow of the American Institute for Medical and Biological Engineering (AIMBE) (conferred in 2007). He received the Outstanding Paper Award from the IEEE UFFC Society (UFFC-S) for two of his papers published in the IEEE Transactions on Ultrasonics, Ferroelectrics, and Frequency Control (TUFFC) in 1992 for the discovery of X wave that, in theory, is both diffraction and dispersion free. Both phase and group velocities of the X wave are faster than the speed of sound (supersonic) or light in vacuum (superluminal) (see newly-developed superluminal X wave in quantum mechanics in 2023 at IEEE TechRxiv <https://doi.org/10.36227/techrxiv.22083719.v2> and 2023 IEEE IUS <https://doi.org/10.1109/IUS51837.2023.10306675>). In addition, he received the Edward C. Kendall Award for his meritorious research from the Mayo Alumni Association in 1992, the NIH FIRST Award in 1991, the Distinguished Service Award from UFFC-S in 2016, and the Engineer of the Year Award from the IEEE Toledo Section in 2021.

Dr. Lu served as the President of IEEE UFFC-S from 2014 to 2015, the Editor-in-Chief of IEEE TUFFC from 2002 to 2007, the General Chair of the 2008 IEEE International Ultrasonics Symposium (IUS), the Technical Program Committee (TPC) Chair of 2001 IEEE IUS, a member of the Editorial Board of IEEE Access from 2016 to 2021, an Elected AdCom member of IEEE UFFC-S from 2009 to 2011, and many committees of UFFC-S. In addition, he served in IEEE Toledo Section.